Model and Control of R-Soft Inverted Pendulum

Daniele Caradonna, Michele Pierallini, *Graduate Student Member, IEEE*, Cosimo Della Santina, *Senior Member, IEEE*, Franco Angelini, *Member, IEEE*, and Antonio Bicchi, *Fellow, IEEE*

***Abstract*—Soft robots enable safe and robust operations in unstructured environments. However, the nonlinearities of their continuum structure complicate the accomplishment of classic robotic tasks, such as pick and place. In this letter, we propose the R-Soft Inverted Pendulum, a Soft Inverted Pendulum (SIP) actuated only by a revolute joint at the base. The objective is to exploit the snap effect to execute pick and place task. We model the proposed system with two approaches: Curvature Parametrization and Strain Parametrization. The former is particularly simple and easy to implement in the classic dynamics of a rigid manipulator, although it suffers from numerical issues. The latter is more complex but guarantees numerical robustness. Additionally, we analyze the equilibria of the system and its structural properties. Furthermore, we propose a control law based on feedback linearization. Finally, we validate the proposed system through simulations.**

***Index Terms*—Modeling, control, and learning for soft robots, underactuated robots.**

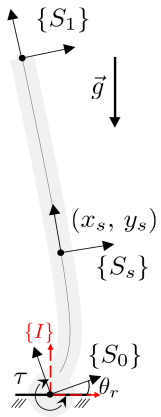

Fig. 1. Scheme of R-Soft Inverted Pendulum (R-SIP), the inherently underactuated soft robotic system whose dynamics and control we characterize in depth in this work.

I. Introduction

SOFT robots [1] represent a paradigm shift in robotic systems due to their inherent characteristics of continuous deformability. The configuration space of soft robots is theoretically infinite [2], meaning the robot tip can reach every point in its workspace with an infinite number of configurations. Soft robots can adapt their shape to nonlinear paths and access difficult-to-reach remote environments [3]. These capabilities empower soft robots to accomplish delicate tasks in unstructured environments and to investigate novel manipulation possibilities. Moreover, the flexibility of their materials makes them well-suited for applications requiring safer physical human–robot interaction.

These properties make modeling and controlling very complex, due to the necessity of managing all the strain modes and the infinite Degrees of Freedom (DoF). As a consequence, achieving easy and well-known robotic tasks, such as pick and place, becomes very challenging.

In the perspective of accomplishing the aforementioned task, we propose a new template model that both exploits the nonlinear behavior of soft structures and eases the integration of soft robots with rigid manipulators (e.g., as an end-effector). In particular, the proposed system is an extension of the Soft Inverted Pendulum (SIP) [2], in which the soft segment is actuated only by a revolute joint at the base. SIP has been previously shown to exhibit the snap effect, i.e., a rapid discharge of stored energy, manifesting a catapult-like trajectory [2], [4]. Therefore, the main idea is to exploit the snap effect to accomplish the pick and place task. The major contribution of this work is the novel template model of R-SIP, accompanied by an analysis of equilibria and structural properties, i.e., stability and controllability. This model is derived using two discretization methods, i.e., Curvature Parametrization [5] and Strain Parametrization [6], [7], which are then compared based on (i) numerical robustness, (ii) computational efficiency, and (iii) accuracy. It is worth stressing here that these two strategies differ only in the formalism used and - consequently - in the way in which the *same* derivations are carried on. In essence, when SP is restricted to the polynomial

Manuscript received 21 November 2023; accepted 21 March 2024. Date of publication 16 April 2024; date of current version 22 April 2024. This letter was recommended for publication by Associate Editor F. Renda and Editor C. Laschi upon evaluation of the reviewers' comments. This work was supported in part by the European Union's Horizon 2020 Research and Innovation Programme under Grant 871237 (SOPHIA), Grant 101016970 (Natural Intelligence), and Grant 101017274 (DARKO), in part by Ministry of University and Research (MUR) as part of the PON 2014-2021 in par by "Research and Innovation" resources – Green/Innovation Action - DM MUR under Grant 1062/2021, and in part by the Italian Ministry of Education and Research in the framework of the "FoReLab" (Future-oriented Research Lab) Project (Departments of Excellence). *(Corresponding author: Daniele Caradonna.)*

Daniele Caradonna is with The BioRobotics Institute and Department of Excellence in Robotics, Scuola Superiore Sant'Anna, 56127 Pisa, Italy (e-mail: daniele.caradonna@santannapisa.it).

Michele Pierallini and Franco Angelini are with the Centro di Ricerca "Enrico Piaggio", Università di Pisa, 56126 Pisa, Italy, and also with the Dipartimento di Ingegneria dell'Informazione, Università di Pisa, 56126 Pisa, Italy.

Cosimo Della Santina is with the Department of Cognitive Robotics, Delft University of Technology, 2628 CN Delft, The Netherlands, and also with the Institute of Robotics and Mechatronics, German Aerospace Center (DLR), 82234 Oberpfaffenhofen, Germany.

Antonio Bicchi is with the Centro di Ricerca "Enrico Piaggio", Università di Pisa, 56126 Pisa, Italy, also with the Dipartimento di Ingegneria dell'Informazione, Università di Pisa, 56126 Pisa, Italy, and also with the Soft Robotics for Human Cooperation and Rehabilitation, Fondazione Istituto Italiano di Tecnologia, 16163 Genova, Italy.

This letter has supplementary downloadable material available at https://doi.org/10.1109/LRA.2024.3389348, provided by the authors.

Digital Object Identifier 10.1109/LRA.2024.3389348

curvature case, these two procedures are two ways to look at exactly the same model.

To our knowledge, this is the first time R-SIP has been modeled with Strain parameterization. Furthermore, a relation between the two approaches is provided. Additionally, we propose a model-based controller and a novel strategy to accomplish the pick-and-place task by exploiting the snap effect. Finally, we validate our model, controller, and strategy through simulations.

II. Related Works

There is no golden rule to model Continuum Soft Robots (CSRs). The infinite DoF of a continuum mechanism launch a challenge to the young soft robotics community, in both theoretical and computational terms. In perspective to control and implementation purposes, the researchers propose many model techniques to predict the nonlinear behavior of soft robots, balancing accuracy and computational efficiency. As well explained in [8], we can classify the available models into four classes: (i) Continuum Mechanics models, (ii) Geometrical models, (iii) Discrete material models, and (iv) Surrogate models.

The main concept of Geometrical models is to assume that the deformed shape of the soft body can be described by a specific curve. One of the most famous models in this category is surely Piecewise Constant Curvature (PCC) [9]. The idea is to discretize the length of the elastic rod, assuming that each piece is a circumference arc. Extending this concept, *Della Santina* et al. [5], [10] propose to assume that each piece can be parametrized by a polynomial curvature, which means that each piece is a Generalized Cornu Spiral [11], i.e., a curve with a polynomial curvature. We call these approaches Curvature Parametrization (CP).

An application of this approach is the Soft Inverted Pendulum (SIP) [2], a soft segment which is applied pure torque on the tip. In [2], *Della Santina* assumes that the curvature is an affine function, reducing the dimension of the state space. Despite the approximation, this system shows some interesting phenomena, such as the blue-sky catastrophe [12, Sec. 2.3]. In particular, it occurs when varying the constant input torque, one or more equilibria disappear, after crossing a critical value. This phenomenon is strictly related to the snap effect, as shown in [2] and [4]. Thanks to these properties, the SIP model received a deep study on the equilibria and stability [13] and an experimental validation [14]. A different version of the SIP is proposed in [15], considering a SIP rigidly attached to a passive revolute joint. This version is very similar to the R-SIP, but different from the actuation source.

In another related work [16], the R-SIP is controlled to perform the swing-up task (i.e., reaching straight configuration), with a linear output feedback controller. The control algorithm is based on a discrete model of an Euler-Bernoulli beam [16]. Differently from CP, this discretization technique requires a large number of DoFs to model accurately soft robots.

The CP permits to compute the Equation of Motion with a classical Lagrangian approach like rigid robots [17]. From a control point of view, this is a great advantage, allowing the use of standard controllers like Feedback Linearization [18]. However, when the curvature goes to zero (straight configuration), the model suffers from numerical issues. Furthermore, the CP gives us only a 2D model of the soft segment and considers only bending as strain mode.

Researchers propose models based on the Cosserat Rod Theory (CRT) to avoid numerical problems and consider all strain modes. In [19], *Renda* et al. discuss the application of CRT to soft robotics, and its formulation via the Lie Group on $SE(3)$. *Grazioso* et al. [3] proposed a CRT-based model with a new discretization technique inspired by the Finite Element Method (FEM). This method assumes that each soft segment is a helix with constant curvature and torsion. *Renda* et al. [20] proposed the Piecewise Constant Strain (PCS) model. This approach aims to parametrize the rod's kinematics with a strain twist, considered constant along the rod. This concept is extended by the works [6], [7], that introduce the Geometric Variable-Strain (GVS). Similar to Polynomial Curvature, the strain twist is generated by a truncated functional basis of space-dependent vectors [8]. Using this method, the user can choose the order of truncation, finding the optimal trade-off in terms of accuracy and computational efficiency. For this reason, this is probably the most accurate and versatile approach. We call these methods Strain Parametrization (SP). GVS method is implemented in a MATLAB toolbox called SoRoSim [21].

III. Modeling R-Soft Inverted Pendulum

The R-Soft Inverted Pendulum is a soft segment actuated only by a revolute joint at the base. In Fig. 1, a representative scheme of R-SIP is shown. This figure also depicts the Systems of Reference (SoR) necessary to define the pose of R-SIP. In particular, let be $\{I\} = \{\boldsymbol{O}_I;\, \boldsymbol{x}_I, \boldsymbol{y}_I, \boldsymbol{z}_I\}$ the inertial frame and $\{S_0\} = \{\boldsymbol{O}_0;\, \boldsymbol{x}_0, \boldsymbol{y}_0, \boldsymbol{z}_0\}$, a frame attached to soft segment's base. With these SoRs, the joint angle $\theta_r(t)$ can be defined as the counterclockwise angle between $\boldsymbol{x}_I$ and $\boldsymbol{x}_0$ axis. The origins of inertial $\{I\}$ and fixed-base $\{S_0\}$ frame are coincident ($\boldsymbol{O}_I - \boldsymbol{O}_0 = \boldsymbol{0}$). The soft segment's length L can be parameterized by the normalized curvilinear abscissa $s \in [0, 1]$. For each point $\bar{s}$, we can define a SoR $\{S_s\}$, described by an homogeneous transformation in $SE(3)$ group. In the case of $\bar{s} = 1$, we define the tip-fixed frame as $\{S_1\} = \{O_1;\, x_1, y_1, z_1\}$. In the following, two model formulations will be proposed, following the two methodologies in the works [2], [5] and [6], [7], for CP and SP, respectively. Note that these two formulations represent the same dynamical system - modulo approximations.[1]

A. Curvature Parametrization

The Curvature Parametrization (CP) describes the pose of a single soft segment by its curvature $\kappa(s, t) : [0, 1] \times \mathbb{R} \to \mathbb{R}$. This statement is valid by making the following assumptions:

1) The soft segment can be considered as a Rod ($L >> D$) [5], [8], [19], [22], where D is the diameter of the soft segment,
2) *Elongation*, *Shear* and *Torsion* strain modes are neglected,
3) The backbone curve associated with the system lives in the 2D plane. This means that we have to consider only the bending around the z axis.

[1]More specifically, we include Magnus expansion as a way of dealing with integrals arising from the derivations in the SP case, which in turn will result in some approximation errors in the end. In principle, this approximation could be used also in the CP case.

Under these assumptions, the pose of the soft segment is completely described by the curvature of the backbone curve. Assuming the curvature as an analytic function, it can be expressed as an infinite sum of monomials [5], i.e.,

$$\kappa(s,t) = \sum_{i=0}^{\infty} \theta_i(t) s^i = \theta_0(t) + \theta_1(t)s + \theta_2(t)s^2 + \dots \quad (1)$$

In (1), the infinite DoF of a continuum soft segment are taken into account.

1) Forward Kinematics: The 2D pose of a generic $\{S_s\}$, w.r.t. $\{S_0\}$, is completely described by its curvature $\kappa(s,t)$, as can be demonstrated by (2) and (3).

$$\alpha_s^0(t) = \int_0^s \kappa(v,t)\, dv = \sum_{i=0}^{\infty} \theta_i(t) \frac{s^{i+1}}{i+1}\,, \quad (2)$$

$$\begin{bmatrix} x_s(t) \\ y_s(t) \end{bmatrix} = \int_0^s \begin{bmatrix} -\sin(\alpha_v^0(t)) \\ +\cos(\alpha_v^0(t)) \end{bmatrix} dv\,. \quad (3)$$

To avoid infinite dimension state space, the curvature can be approximated as an affine function in s [2], i.e.,

$$\kappa(s,t) \simeq \theta_0(t) + \theta_1(t)s\,. \quad (4)$$

With (4), the 2D pose of a single segment can be expressed in closed-form equations. In fact, with $\alpha_s^0 = \theta_0\, s + \theta_1 \frac{s^2}{2}$, 2D position can be written as $x_s(\frac{\theta_0^2}{2\theta_1}, \frac{\theta_0+s\theta_1}{\sqrt{\pi\theta_1}})$ and $y_s(\frac{\theta_0^2}{2\theta_1}, \frac{\theta_0+s\theta_1}{\sqrt{\pi\theta_1}})$, where the complete expressions can be found in [2].

Despite the 2D position being well-defined for $(\theta_0, \theta_1) \to 0$ [2], the computation of Forward Kinematics suffers from numerical issues in the neighborhood of the straight configuration (i.e., $\theta_0 = \theta_1 = 0$).

A s-fixed frame $\{S_s\}$ pose, w.r.t. $\{S_0\}$, can be described by $\boldsymbol{T}_s^0 \in SE(3)$, defined as

$$\boldsymbol{T}_s^0 = \begin{bmatrix} \boldsymbol{R}_z\left(\alpha_s^0\right) & \boldsymbol{p}_s \\ \boldsymbol{0}^T & 1 \end{bmatrix}, \quad (5)$$

where $\boldsymbol{p}_s = \begin{pmatrix} x_s & y_s & 0 \end{pmatrix}^\top$ and $\boldsymbol{R}_z(\cdot) \in SO(3)$ is the elementary rotation matrix around z-axis. In addition, the pose of $\{S_0\}$ can be written w.r.t. $\{I\}$ through $\boldsymbol{T}_0^I(\theta_\mathrm{r}) \in SE(3)$, that represents a pure rotation around z-axis. Similarly to length, thickness D can be parameterized by $d \in [-\frac{1}{2}, \frac{1}{2}]$. Finally, a point of the soft segment, at length s and thickness d, can be expressed in Inertial Frame as:

$$\boldsymbol{p}_{sd}^I = \boldsymbol{R}_z(\theta_\mathrm{r})\, \boldsymbol{p}_s + \boldsymbol{R}_z(\theta_\mathrm{r} + \alpha_s^0) \begin{bmatrix} dD & 0 & 0 \end{bmatrix}^\top. \quad (6)$$

Equation (6) is the Forward Kinematics of R-SIP with CP.

2) Differential Kinematics: Let $\boldsymbol{q} = \begin{bmatrix} \theta_\mathrm{r} & \theta_0 & \theta_1 \end{bmatrix}^\top \in \mathbb{R}^3$ be the generalized joint vector. From (6), Differential Kinematics can be easily computed. The Jacobian matrix $\boldsymbol{J}_{sd}^I$ maps the joint velocity vector $\dot{\boldsymbol{q}}$ in the linear velocity $\dot{\boldsymbol{p}}_{sd}^I$:

$$\dot{\boldsymbol{p}}_{sd}^I = \boldsymbol{J}_{sd}^I(\boldsymbol{q})\, \dot{\boldsymbol{q}}\,. \quad (7)$$

The Jacobian matrix can be computed by derivation ($\boldsymbol{J}_{sd}^I(\boldsymbol{q}) = \nabla_{\boldsymbol{q}}(x_{sd}^I, y_{sd}^I)$), obtaining such as written below,

$$\boldsymbol{J}_{sd}^I(\boldsymbol{q}) = \begin{bmatrix} \left(\boldsymbol{R}_z(\frac{\pi}{2} + \theta_\mathrm{r})\right) \boldsymbol{p}_{sd} & \boldsymbol{R}_z(\theta_\mathrm{r}) \boldsymbol{J}_{sd}(\theta_0,\, \theta_1) \end{bmatrix}, \quad (8)$$

where $\boldsymbol{J}_{sd}$ is the Jacobian derived in [2].

3) Dynamics: Applying the classical Lagrangian approach for rigid manipulators [17], it is possible to derive dynamics. The Equations of Motion (EoM) can be finally written as:

$$\boldsymbol{M}(\boldsymbol{q})\ddot{\boldsymbol{q}} + \boldsymbol{C}(\boldsymbol{q}, \dot{\boldsymbol{q}})\dot{\boldsymbol{q}} + \boldsymbol{G}(\boldsymbol{q}) + \boldsymbol{K}(\boldsymbol{q}) + \boldsymbol{D}(\boldsymbol{q}, \dot{\boldsymbol{q}}) = \boldsymbol{S}^\top \tau\,, \quad (9)$$

where $\boldsymbol{S} = \begin{bmatrix} 1 & 0 & 0 \end{bmatrix}$, $\boldsymbol{M}(\boldsymbol{q}) \in \mathbb{R}^{3\times3}$ is the inertia matrix, $\boldsymbol{C}(\boldsymbol{q}, \dot{\boldsymbol{q}}) \in \mathbb{R}^{3\times3}$ is the Coriolis matrix, $\boldsymbol{G}(\boldsymbol{q}) \in \mathbb{R}^3$ is the gravity vector, $\boldsymbol{K} : \mathbb{R}^3 \to \mathbb{R}^3$ and $\boldsymbol{D} : \mathbb{R}^3 \times \mathbb{R}^3 \to \mathbb{R}^3$ are the stiffness and the damping contributions. Finally, $\tau \in \mathbb{R}$ is the torque input on the revolute joint.

The inertia matrix $\boldsymbol{M}(\boldsymbol{q})$ can be computed by kinetic energy, resulting in

$$\boldsymbol{M}(\boldsymbol{q}) = \int_0^1 \int_{-\frac{1}{2}}^{\frac{1}{2}} \rho(s,d)\, {\boldsymbol{J}_{sd}^I}^\top \boldsymbol{J}_{sd}^I \,\mathrm{d}d\,\mathrm{d}s\,, \quad (10)$$

where $\rho(s,d)$ is the density of soft segment. $\boldsymbol{M}(\boldsymbol{q})$ can rewritten in block matrices

$$\boldsymbol{M}(\boldsymbol{q}) = \begin{bmatrix} M_{11}(\theta_0,\theta_1) & \boldsymbol{M}_{12}(\theta_0,\theta_1) \\ \boldsymbol{M}_{12}^\top(\theta_0,\theta_1) & \boldsymbol{M}_{22}(\theta_0,\theta_1) \end{bmatrix}, \quad (11)$$

where $\boldsymbol{M}_{22}$ is the inertia matrix of SIP, found in [2]. It is important to highlight that the inertia matrix is independent of θ_r and depends only on the soft segment's configuration (θ_0, θ_1). Furthermore, in the case of uniform density ($\rho(s,d) = \bar{\rho}$) or mass concentrated on the tip ($\rho(s,d) = \bar{\rho}\,\delta(s-1)$), this integral has an analytic solution [2].

The gravity vector $\boldsymbol{G}(\boldsymbol{q})$ is defined as gradient of gravitational potential energy ($\boldsymbol{G}(\boldsymbol{q}) = \nabla_{\boldsymbol{q}}\mathcal{U}(\boldsymbol{q})$), as written below.

$$\mathcal{U}(\boldsymbol{q}) = \int_0^1 \int_{-\frac{1}{2}}^{\frac{1}{2}} \rho g \left(\mathrm{s}_{\phi+\theta_r} x_{sd} + \mathrm{c}_{\phi+\theta_r} y_{sd}\right) \mathrm{d}d\,\mathrm{d}s \quad (12)$$

In (12), ϕ is the inclination of the gravitation field w.r.t the frame $\{I\}$. In our case, we assume that there is no relative inclination ($\phi = 0$).

The Coriolis matrix $\boldsymbol{C}(\boldsymbol{q}, \dot{\boldsymbol{q}})$ is computed using classical derivation for rigid kinematic chains [17].

Under the assumption of perfectly viscoelastic material [22], the stiffness and damping contributions can be supposed linear, such as $\boldsymbol{K}(\boldsymbol{q}) = \boldsymbol{K}\boldsymbol{q}$ and $\boldsymbol{D}(\boldsymbol{q}, \dot{\boldsymbol{q}}) = \boldsymbol{D}\dot{\boldsymbol{q}}$. In particular, $\boldsymbol{K} \in \mathbb{R}^{3\times3}$ and $\boldsymbol{D} \in \mathbb{R}^{3\times3}$ are constant matrices, defined as

$$\boldsymbol{K} = \mathrm{diag}\left(k_\mathrm{r},\, k\boldsymbol{H}\right), \quad \boldsymbol{D} = \mathrm{diag}\left(\beta_\mathrm{r},\, \beta\boldsymbol{H}\right), \quad (13)$$

where $\boldsymbol{H} \in \mathbb{R}^{2\times2}$ is the Hankel matrix. k, β are the stiffness and damping coefficients of the soft segments, meanwhile k_r, and β_r are the stiffness and damping coefficients of the revolute joint.

Finally, the general input field can be computed as the sum of two contributions. The former corresponds to the active torque applied by the revolute joint. The latter is related to the soft actuators embedded in the soft segments (e.g., pneumatic actuators), modeled as pure torques.

If n_a is the total number of actuators and $s_{\mathrm{a},j}$ is the point at which the j-th soft actuator applies the active torque, the general input field can be computed as

$$\underbrace{\boldsymbol{S}^\top \tau}_{\text{Rev. Joint}} + \sum_{j=1}^{n_\mathrm{a}} \underbrace{\boldsymbol{A}_R\left(s_{\mathrm{a},j}\right) \tau_j}_{j\text{-th Soft Actuator}}, \quad \boldsymbol{A}_R\left(s_{\mathrm{a},j}\right) = \begin{bmatrix} 1 \\ \boldsymbol{A}\left(s_{\mathrm{a},j}\right) \end{bmatrix}, \quad (14)$$

where τ_j is the magnitude of the j-th soft actuator (e.g., pressure, tension), $\boldsymbol{A}(s_\mathrm{a}) = (\frac{s_\mathrm{a}^{i+1}}{i+1})_{i=0}^{n-1}$ is the input field derived in [2], and

n is the number of coefficients of the polynomial curvature. The matrix $\boldsymbol{A}_R(s_\mathrm{a})$ in (14) is the transpose of orientation Jacobian, such as $(\dot{\theta}_\mathrm{r} + \dot{\alpha}_s^0) = \boldsymbol{A}_R^\top(s)\,\dot{\boldsymbol{q}}$. In our case, there are no embedded soft actuators, resulting in an input field with only the revolute joint contribution, as already shown in (9).

B. Strain Parametrization

Strain Parametrization (SP) is based on Cosserat Rod Theory (CRT) [22], which describes the dynamics of a hyperelastic rod with a set of Partial Differential Equations (PDEs). To solve kinematics, this formulation uses Lie Algebra, a mathematical tool well known in classical robotics literature [23]. SP describes the 3D pose of a rod through strain twist $\boldsymbol{\xi}(X,t) \in \mathbb{R}^6$, defined as

$$\boldsymbol{\xi}(X,t) = \left(\boldsymbol{g}^{-1}\,\boldsymbol{g}'\right)^\vee\,, \quad \boldsymbol{\xi}(X,t) = \begin{bmatrix}\boldsymbol{\xi}_\kappa^\top & \boldsymbol{\xi}_\sigma^\top\end{bmatrix}^\top\,, \tag{15}$$

where $X = sL$ is the material abscissa and $\boldsymbol{g}(X,t) \in SE(3)$ describes the configuration of a cross-section s respect to $\{S_0\}$. The strain field can be considered as generated by a finite functional basis of strain modes [6], [7]

$$\boldsymbol{\xi}(X,t) = \boldsymbol{B}_\xi(X)\,\boldsymbol{q}_\xi(t) + \boldsymbol{\xi}^*\,, \tag{16}$$

where $\boldsymbol{B}_\xi \in \mathbb{R}^{6\times n}$ is a matrix function whose columns form the basis of the strain field, $\boldsymbol{q}_\xi \in \mathbb{R}^n$ is the vector of coordinates in that basis, and $\boldsymbol{\xi}^* \in \mathbb{R}^6$ is the reference strain. Following the analogy with polynomial curvature [5], $\boldsymbol{B}_\xi$ is usually supposed polynomial. To have a model comparable with the one obtained previously (9), here we assume no elongation, torsion, or shear modes. Under these assumptions, we can write the strain field of R-SIP as:

$$\boldsymbol{\xi} = \begin{bmatrix}\boldsymbol{0}_{5\times1} & \boldsymbol{0}_{5\times1}\\ 1 & X\end{bmatrix}\begin{bmatrix}q_0\\ q_1\end{bmatrix} + \begin{bmatrix}1\\ \boldsymbol{0}_{5\times1}\end{bmatrix} = \begin{bmatrix}1\\ \boldsymbol{0}_{4\times1}\\ q_0 + q_1 X\end{bmatrix}\,. \tag{17}$$

In (17), we set a first-order polynomial to keep the analogy with the affine curvature of SIP.

1) Forward Kinematics: It is possible to compute the Forward Kinematics of R-SIP as a product of exponentials

$$\boldsymbol{g}^I(X,t) = \exp_{SE(3)}\left(\hat{\boldsymbol{\xi}}_R\,\theta_\mathrm{r}\right)\,\exp_{SE(3)}\left(\hat{\boldsymbol{\Omega}}(X,t)\right)\,, \tag{18}$$

where $\hat{\boldsymbol{\Omega}}(X,t) \in \mathfrak{se}(3)$ is the Magnus Expansion [24] of $\boldsymbol{\xi}(X)$ at the point X and $\boldsymbol{\xi}_R \in \mathbb{R}^6$ is the twist associated to the revolute joint, such that

$$\exp_{SE(3)}\left(\hat{\boldsymbol{\xi}}_R\,\theta_\mathrm{r}\right) = \boldsymbol{T}_0^I(\theta_\mathrm{r})\,. \tag{19}$$

Defined $\boldsymbol{q} = \begin{bmatrix}\theta_\mathrm{r} & \boldsymbol{q}_\xi^\top\end{bmatrix}^\top \in \mathbb{R}^3$ as generalized joint variables vector, (18) can be considered the Forward Kinematics of R-SIP with SP. It is worth highlighting that (18) does not suffer from numerical issues in the case of $\boldsymbol{q}_{\boldsymbol{\xi}} \to 0$, instead of CP.

2) Differential Kinematics: Let $\boldsymbol{\eta}^r(X) \in \mathbb{R}^6$ be the relative velocity twist associated with the soft segment, defined as

$$\hat{\boldsymbol{\eta}}^r = \boldsymbol{g}^{-1}\dot{\boldsymbol{g}}\,. \tag{20}$$

Strain and velocity twist are related by the equality of mixed partial derivatives

$$\boldsymbol{\eta}^{r\prime} = \dot{\boldsymbol{\xi}} - \mathrm{ad}_{\boldsymbol{\xi}}\,\boldsymbol{\eta}^r\,. \tag{21}$$

Integrating (21), it is possible to express the relative velocity twist in the function of $\dot{\boldsymbol{q}}_\xi$.

$$\boldsymbol{\eta}^r(X,t) = \left(\mathrm{Ad}_{\boldsymbol{g}}^{-1}\int_0^X \mathrm{Ad}_{\boldsymbol{g}}\boldsymbol{B}_\xi\,\mathrm{d}\zeta\right)\dot{\boldsymbol{q}}_\xi \tag{22}$$

The absolute velocity twist, expressed in the local frame can be computed as

$$\boldsymbol{\eta}(X,t) = \mathrm{Ad}_{\boldsymbol{g}}^{-1}\,\boldsymbol{\xi}_R\,\dot{\theta}_\mathrm{r} + \boldsymbol{\eta}^r(X,t)\,. \tag{23}$$

Finally, we can obtain the *Soft Geometric Jacobian* as:

$$\boldsymbol{\eta} = \mathrm{Ad}_{\boldsymbol{g}}^{-1}\begin{bmatrix}\boldsymbol{\xi}_R & \int_0^X \mathrm{Ad}_{\boldsymbol{g}}\boldsymbol{B}_\xi\,\mathrm{d}\zeta\end{bmatrix}\begin{bmatrix}\dot{\theta}_\mathrm{r}\\ \dot{\boldsymbol{q}}_\xi\end{bmatrix} = \boldsymbol{J}(\boldsymbol{q})\dot{\boldsymbol{q}}\,. \tag{24}$$

3) Dynamics: Dynamics equations of R-SIP can be computed using D'Alembert's principle:

$$\boldsymbol{M}(\boldsymbol{q})\ddot{\boldsymbol{q}} + \boldsymbol{C}(\boldsymbol{q},\dot{\boldsymbol{q}})\dot{\boldsymbol{q}} + \boldsymbol{G}(\boldsymbol{q}) + \boldsymbol{K}\boldsymbol{q} + \boldsymbol{D}\dot{\boldsymbol{q}} = \boldsymbol{S}^\top\tau\,. \tag{25}$$

Similarly to (9), the stiffness and damping contributions are computed assuming a linear viscoelastic constitutive law [6]. The dynamics matrices can be written as:

- *Inertia Matrix* $\boldsymbol{M}(\boldsymbol{q}) \in \mathbb{R}^{3\times3}$:

$$\boldsymbol{M}(\boldsymbol{q}) = \int_0^L \boldsymbol{J}^\top\boldsymbol{\mathcal{M}}\boldsymbol{J}\,\mathrm{d}X\,, \tag{26}$$

- *Gravity Vector* $\boldsymbol{G}(\boldsymbol{q}) \in \mathbb{R}^3$:

$$\boldsymbol{G}(\boldsymbol{q}) = \int_0^L \boldsymbol{J}^\top\boldsymbol{\mathcal{M}}\left(\mathrm{Ad}_{\boldsymbol{g}^I}^{-1}\,\boldsymbol{\mathcal{G}}\right)\,\mathrm{d}X\,, \tag{27}$$

  where $\boldsymbol{\mathcal{G}} \in \mathbb{R}^6$ is the gravitational acceleration twist, expressed in the inertial frame.
- *Coriolis Matrix* $\boldsymbol{C}(\boldsymbol{q},\dot{\boldsymbol{q}}) \in \mathbb{R}^{3\times3}$:

$$\boldsymbol{C}(\boldsymbol{q},\dot{\boldsymbol{q}}) = \int_0^L \boldsymbol{J}^\top\left(\mathrm{ad}_{\boldsymbol{\eta}}^*\boldsymbol{\mathcal{M}}\boldsymbol{J} + \boldsymbol{\mathcal{M}}\dot{\boldsymbol{J}}\right)\,\mathrm{d}X\,, \tag{28}$$

- *Stiffness Matrix* $\boldsymbol{K} \in \mathbb{R}^{3\times3}$:

$$\boldsymbol{K} = \begin{bmatrix}k_\mathrm{r} & \boldsymbol{0}\\ \boldsymbol{0} & \int_0^L \boldsymbol{B}_\xi^\top\boldsymbol{\Sigma}\,\boldsymbol{B}_\xi\,\mathrm{d}X\end{bmatrix}\,, \tag{29}$$

- *Damping Matrix* $\boldsymbol{D} \in \mathbb{R}^{3\times3}$:

$$\boldsymbol{D} = \begin{bmatrix}\beta_\mathrm{r} & \boldsymbol{0}\\ \boldsymbol{0} & \int_0^L \boldsymbol{B}_\xi^\top\boldsymbol{\Upsilon}\,\boldsymbol{B}_\xi\,\mathrm{d}X\end{bmatrix}\,, \tag{30}$$

where $\boldsymbol{\mathcal{M}} = \rho\,\mathrm{diag}(A\,\boldsymbol{I}_{3\times3}, J_x, J_y, J_z) \in \mathbb{R}^{6\times6}$, $\boldsymbol{\Sigma} = \mathrm{diag}\,(E\,A, G\,A, G\,A, G\,J_x, E\,J_y, E\,J_z) \in \mathbb{R}^{6\times6}$ and $\boldsymbol{\Upsilon} = \beta\,\mathrm{diag}\,(3\,A, A, A, J_x, 3\,J_y, 3\,J_z) \in \mathbb{R}^{6\times6}$. Here, A is the cross-sectional area, J_i is the second moment of area around the axis i, E is the Young Modulus, and G is the shear modulus.

Equations (26)-(29) are derived from the works [6], [7]. EoM derived with GVS (25) are expressed in the classical Lagrangian form, useful for control purposes.

C. Structural Properties

1) Equilibria and Stability: For an exhaustive study of the system, it is mandatory to study the equilibria and their stability.

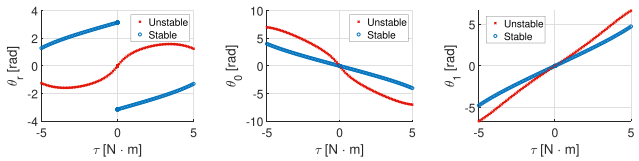

(a) θ_r w.r.t. τ. (b) θ_0 w.r.t. τ. (c) θ_1 w.r.t. τ.

Fig. 2. Equilibria of R-SIP, founded varying $\bar{\tau}$. Unstable and stable equilibria are, respectively, red crosses and blue circles.

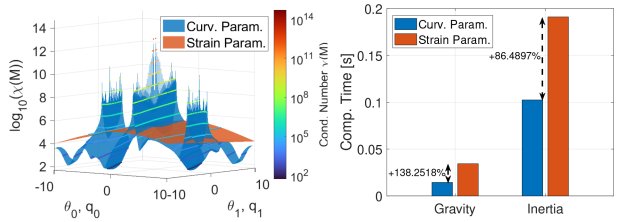

(a) Condition Numbers. (b) Computational Time.

Fig. 3. Comparison between the two models. In (a) is shown the Condition Number of Inertia Matrix $\boldsymbol{M}(\boldsymbol{q})$, respectively in the CP (blue) and SP (orange) case. In (b), is shown a comparison in terms of computational time.

The equilibria equation can be derived from (9) or (25), imposing $\ddot{\boldsymbol{q}} = \dot{\boldsymbol{q}} = \boldsymbol{0}$ and a constant input $\tau = \bar{\tau}$ [25], which leads to

$$\boldsymbol{G}(\bar{\boldsymbol{q}}) + \boldsymbol{K}(\bar{\boldsymbol{q}}) = \boldsymbol{S}^\top \bar{\tau}\,. \tag{31}$$

In this work, we suppose no stiffness on the revolute joint ($k_r = 0$). The solutions $\bar{\boldsymbol{q}}$ of (31), varying constant torque in the range $\bar{\tau} \in [-5,\ 5]$ Nm, are represented in Fig. 2(a)–(c).

The stability of these equilibria can be determined thanks to the Lyapunov Direct Theorem. In particular, an equilibrium is asymptotically stable if [26]

$$\boldsymbol{\mathcal{K}} = \left(\frac{\partial \boldsymbol{K}(\boldsymbol{q})}{\partial \boldsymbol{q}} + \frac{\partial \boldsymbol{G}(\boldsymbol{q})}{\partial \boldsymbol{q}} \right)_{|_{\boldsymbol{q}=\bar{\boldsymbol{q}}}} \succ \boldsymbol{0}\,, \tag{32}$$

where "$\succ 0$" means that the matrix is positive definite. Equation (32) can be particularized with the linear stiffness contribution (13) or (29), resulting in $\partial \boldsymbol{K}(\boldsymbol{q})/\partial \boldsymbol{q} = \boldsymbol{K}$. Given that $\boldsymbol{K} \succ 0$, the term $\frac{\partial \boldsymbol{G}(\boldsymbol{q})}{\partial \boldsymbol{q}}$ results crucial for stability. The proof of this theorem can be found in [26]. In Fig. 2, unstable equilibria are indicated as red and stable ones in blue. In the same fashion of [2], we studied also equilibria varying stiffness k, in the case of the autonomous system $\bar{\tau} = 0$, resulting in two Pendulum-like equilibria, that are independent from the stiffness k, i.e.,

$$\bar{\boldsymbol{q}}^{(1)} = \begin{bmatrix} 0 & 0 & 0 \end{bmatrix}^\top, \qquad \bar{\boldsymbol{q}}^{(2)} = \begin{bmatrix} \pm\pi & 0 & 0 \end{bmatrix}^\top. \tag{33}$$

Substituting (33) in (32), we can deduce their stability.

$$\boldsymbol{\mathcal{K}}(\bar{\boldsymbol{q}}^{(1),(2)}) = \begin{bmatrix} \mp Lgm & \mp\frac{1}{2}Lgm & \mp\frac{1}{6}Lgm \\ \mp\frac{1}{2}Lgm & k \mp \frac{1}{3}Lgm & \frac{k}{2} \mp \frac{1}{8}Lgm \\ \mp\frac{1}{6}Lgm & \frac{k}{2} \mp \frac{1}{8}Lgm & \frac{k}{3} \mp \frac{1}{20}Lgm \end{bmatrix} \tag{34}$$

From $\boldsymbol{\mathcal{K}}(\bar{\boldsymbol{q}}^{(1)})$, we can see that the matrix is not positive definite, $\forall k$, and from $\boldsymbol{\mathcal{K}}(\bar{\boldsymbol{q}}^{(2)})$ we can see that the matrix is positive definite, $\forall k$. Autonomous R-SIP, in contrast to SIP, does not show *blue-sky catastrophe* and *Supercritical pitchfork bifurcation*. For further details on this latter phenomenon, see [12, Sec. 2.3]. Apparently, the revolute joint cancels these nonlinear and elastic properties.

2) Controllability: The R-SIP is an under-actuated system with 1 active DoF (i.e., θ_r) and 2 passive DoFs (i.e., $\theta_0\,, \theta_1$ for CP and $q_0\,, q_1$ for SP). According to [18], the system is not *strongly inertially coupled*, since the number of active DoFs is less than the passive DoFs. For this reason, it is mandatory to check the controllability of the system. In the first analysis, we check the controllability of the linearized system.

$$\begin{bmatrix} \dot{\boldsymbol{q}} \\ \ddot{\boldsymbol{q}} \end{bmatrix} = \underbrace{\begin{bmatrix} \boldsymbol{0}_{3\times3} & \boldsymbol{I}_{3\times3} \\ \boldsymbol{A}_{21} & \boldsymbol{A}_{22} \end{bmatrix}_{|_{\boldsymbol{q}=\bar{\boldsymbol{q}}}}}_{\boldsymbol{A}} \begin{bmatrix} \boldsymbol{q} \\ \dot{\boldsymbol{q}} \end{bmatrix} + \underbrace{\begin{bmatrix} \boldsymbol{0}_{3\times1} \\ \boldsymbol{M}^{-1}\boldsymbol{S}^\top \end{bmatrix}_{|_{\boldsymbol{q}=\bar{\boldsymbol{q}}}}}_{\boldsymbol{B}} \bar{\tau} \tag{35}$$

where $\boldsymbol{A}_{21} = -\boldsymbol{M}^{-1}\boldsymbol{\mathcal{K}}$ and $\boldsymbol{A}_{22} = -\boldsymbol{M}^{-1}\boldsymbol{D}$.

Rewriting (35) in state space form, we can check the controllability of the system by the rank of the controllability matrix

$$\boldsymbol{\mathcal{R}} = \begin{bmatrix} \boldsymbol{B} & \boldsymbol{AB} & \boldsymbol{A}^2\boldsymbol{B} & \dots & \boldsymbol{A}^5\boldsymbol{B} \end{bmatrix}. \tag{36}$$

In particular, the system results small-time locally controllable in $\bar{q}$, for every equilibria found in this section.

D. Comparison of the Two Approaches

Despite representing the same dynamical systems, the two ways discussed to derive the proposed models of the R-SIP (9), (25) show different properties.

1) Numerical Issues: In CP, forward kinematics suffers from numerical issues, as highlighted in Section III-A. These issues also afflict dynamics equations (9). In particular, inertia matrix (10) shows a maximum condition number $\chi_{\max} \approx 10^{14}$ in a neighborhood of the origin, shown in Fig. 3(a). On the contrary, in SP, forward kinematics (18) is well-conditioned, thanks to the product of exponential matrices. The condition number of inertia matrix (26) is represented in Fig. 3(a) and reaches a maximum condition number of $\chi_{\max} \approx 10^5$.

2) Computational Cost: : In CP, dynamics matrices ($\boldsymbol{M}(\boldsymbol{q})$, $\boldsymbol{G}(\boldsymbol{q})$, etc.) can be computed analytically. In the case of SP, dynamics matrices have to be computed numerically due to Magnus Expansion of strain twist $\boldsymbol{\xi}(X,t)$. This fact impacts negatively on the computational cost of the dynamics matrices, necessary for model-based controllers. In the case of SP, the computational time of the inertia matrix and gravity vector increase of 86.49% and 138.25%, respectively. In Fig. 3(b), is shown a comparison between the computational times of dynamics matrices, computed with both approaches. The computational times shown in Fig. 3(b) are derived using the MATLAB functions `tic` and `toc`, running on a laptop with an Intel Core i7.

3) Accuracy: SP is surely the most complete and accurate. In the general case, an R-SIP can be modeled in 3D space, including elongation/compression, shear, and torsion modes. This model can be easily extended in a general 3D formulation with all strain modes. On the contrary, the polynomial curvature model permits only 2D motion with only bending mode. Since the two proposed representations of the R-SIP model are equivalent, up to differences in how integrals are solved, it is possible to derive a relation between the two approaches and the two generalized joint variables that describe the curvature and the strain field. As seen in Section III-A, a curve that lives in a plane,

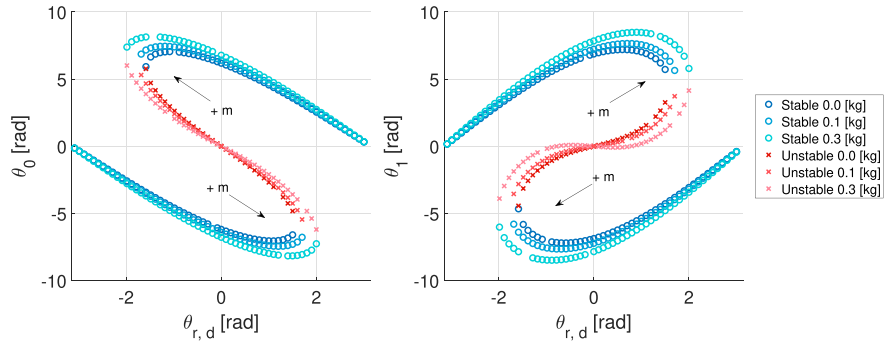

Fig. 4. Equilibria of autonomous SIP, varying θ_{rd}. Unstable and stable equilibria are, respectively, red crosses and blue circles. The equilibria are computed also varying the lumped mass on the tip, representing the mass of the object.

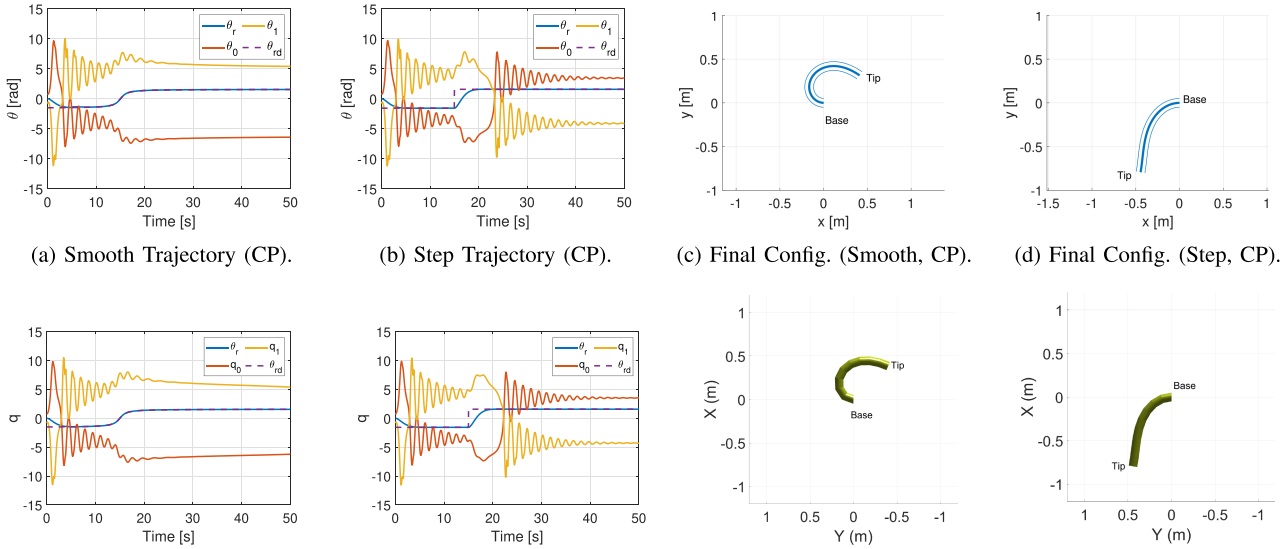

(a) Smooth Trajectory (CP). (b) Step Trajectory (CP). (c) Final Config. (Smooth, CP). (d) Final Config. (Step, CP).

(e) Smooth Trajectory (SP). (f) Step Trajectory (SP). (g) Final Config. (Smooth, SP). (h) Final Config. (Step, SP).

Fig. 5. Simulations with two desired trajectories of R-SIP, modelled with CP (a, b) and SP (e, f). (c, d) and (g, h) show the final configuration of R-SIP of the four simulations.

can be completely defined by its curvature. More precisely, $\kappa(X,t)$ is the *signed curvature*, see [27] for further details. Given that $\alpha(X)$ is the phase of the tangent versor $\boldsymbol{t}(X)$, the signed curvature can be defined as the spatial derivative of the phase of this versor, i.e. $\kappa(X) = \alpha'(X)$.

Remark: In the 2D case, $\xi_{\kappa_z}(X)$ from SP is equal to the curvature $\kappa(X)$ from CP.

$$\xi_{\kappa_z}(X) = \kappa(X)\,. \tag{37}$$

Proof: From the definition of signed curvature, we can write the tangent versor and its derivative:

$$\boldsymbol{t}(X) = \begin{bmatrix}\cos(\alpha)\\ \sin(\alpha)\\ 0\end{bmatrix}, \quad \boldsymbol{t}'(X) = \kappa(X)\begin{bmatrix}-\sin(\alpha)\\ \cos(\alpha)\\ 0\end{bmatrix}. \tag{38}$$

Using Frenet-Serret equations in the 2D case, it is possible to rewrite the derivative of the tangent versor as

$$\boldsymbol{t}'(X) = \boldsymbol{R}_s^0\,\tilde{\boldsymbol{\xi}}_\kappa\,\begin{bmatrix}1 & 0 & 0\end{bmatrix}^\top. \tag{39}$$

Substituting (39) in (38), we obtain the equality

$$\boldsymbol{R}_s^0\begin{bmatrix}0\\ \xi_{\kappa_z}\\ 0\end{bmatrix} = \kappa(X)\begin{bmatrix}-\sin(\alpha)\\ \cos(\alpha)\\ 0\end{bmatrix}. \tag{40}$$

Recalling (40) and the definition of the normal versor, we finally obtain (37).

Substituting $X = sL$, we finally obtain

$$\kappa(s) = \xi_{\kappa_z}(s) \to \sum_{i=0}^{n-1}\theta_i s^i = \sum_{i=0}^{n-1} q_i (sL)^i\,, \tag{41}$$

$$\theta_i = L^i\,q_i \quad i \in [0,\,n-1]\,. \tag{42}$$

Equation (42) shows that the two generalized joint vectors, with the assumptions of SIP [2], differ from each other only by a scale factor.

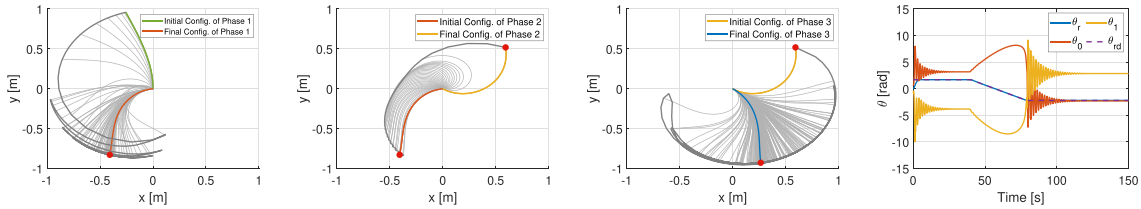

(a) Phase 1. (b) Phase 2. (c) Phase 3. (d) $\boldsymbol{q}$ over time.

Fig. 6. Pick and place planner applied on R-SIP. (a-c) show snapshots of the catapult trajectory, where the red circle represents the object. In particular, (a) is the "pick" point and (c) the "place" point. In (d), the evolution over the time of $\boldsymbol{q}$.

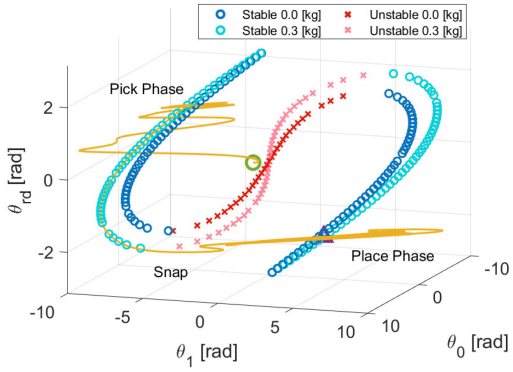

Fig. 7. Evolution of the R-SIP controlled with the pick and place planner, represented in the phase space. In this figure are also shown the equilibria of zero dynamics with $\Delta m = 0$ and $\Delta m = m_{\text{obj}}$, to visualize the pick and place strategy. The green circle shows the initial state $\boldsymbol{q}(0)$ and the purple triangle the final state $\boldsymbol{q}(t_{\text{f}})$.

IV. Control

R-SIP is an under-actuated system, described by (9) or (25). According to [18], we can rewrite the dynamics as:

$$\begin{cases} M_{11}\ddot{\theta}_{\text{r}} + \boldsymbol{M}_{12}\ddot{\boldsymbol{q}}_{\text{sip}} + h_1 + G_1 = \tau \\ \boldsymbol{M}_{12}^{\top}\ddot{\theta}_{\text{r}} + \boldsymbol{M}_{22}\ddot{\boldsymbol{q}}_{\text{sip}} + \boldsymbol{h}_2 + \boldsymbol{G}_2 = \boldsymbol{0} \end{cases}, \tag{43}$$

where $\boldsymbol{h}(\boldsymbol{q}, \dot{\boldsymbol{q}}) = \begin{bmatrix} h_1 & \boldsymbol{h}_2^{\top} \end{bmatrix}^{\top}$ is defined as $\boldsymbol{h}(\boldsymbol{q}, \dot{\boldsymbol{q}}) = \boldsymbol{C}(\boldsymbol{q}, \dot{\boldsymbol{q}})\dot{\boldsymbol{q}} + \boldsymbol{K}\boldsymbol{q} + \boldsymbol{D}\dot{\boldsymbol{q}}$ and $\boldsymbol{q}_{\text{sip}}$ is general coordinates vector that describes soft segment's kinematics, whatever parametrization has been used.

A well-known controller that can be implemented in this system is Collocated Feedback Linearization [18]. The goal is controlling the actuated joint variable θ_{r} to follow a desired trajectory $\theta_{\text{rd}}(t)$. To achieve that, the control law is

$$\begin{aligned} \tau = &\left(M_{11} - \boldsymbol{M}_{12}\boldsymbol{M}_{22}^{-1}\boldsymbol{M}_{12}^{T}\right) v + h_1 + \\ &+ G_1 - \boldsymbol{M}_{12}\boldsymbol{M}_{22}^{-1}\left(\boldsymbol{h}_2 + \boldsymbol{G}_2\right), \end{aligned} \tag{44}$$

where v can be chosen as classical PD controller, with gains that minimize LQR cost function, i.e.,

$$v = \ddot{\theta}_{\text{rd}} + K_D\left(\dot{\theta}_{\text{rd}} - \dot{\theta}_{\text{r}}\right) + K_P\left(\theta_{\text{rd}} - \theta_{\text{r}}\right). \tag{45}$$

The Zero Dynamics of the controlled system is:

$$\boldsymbol{M}_{22}\ddot{\boldsymbol{q}}_{\text{sip}} + \boldsymbol{h}_2(\boldsymbol{q}_{\text{sip}}, \dot{\boldsymbol{q}}_{\text{sip}}) + \boldsymbol{G}_2(\boldsymbol{q}_{\text{sip}}, \theta_{\text{rd}}) = \boldsymbol{0}. \tag{46}$$

Equation (46) represents the dynamics equation of autonomous SIP, as known from [2]. The controlled system converges to equilibrium $(\theta_{\text{rd}}, \bar{q}_{\text{sip}})$, in which $\bar{q}_{\text{sip}}$ depends also by the desired θ_{rd}. The performance of the controlled R-SIP strongly depends on the physical properties of the SIP, as highlighted by (46). For this reason, we can map equilibria of Zero Dynamics varying θ_{rd}, as shown in Fig. 4. The equilibria map is derived considering a varying lumped mass Δm on the robot's tip, in perspective to consider the load applied by the object during the pick and place task.

Considering the equilibria map for $\Delta m = 0$, we notice the occurrence of the blue-sky catastrophe phenomenon, for $|\theta_{\text{rd}}| > \theta^*_{\text{rd}}(0) = \frac{\pi}{2}$. Here, $\theta^*_{\text{rd}}(\Delta m)$ represents the critical angle at which the blue-sky catastrophe arises, varying the object's mass Δm. Therefore, it is possible to exploit the snap effect in the controlled R-SIP system, overcoming the impossibility of an autonomous R-SIP to show this phenomenon. In [4], the Authors found a similar equilibria map in which the critical value corresponds to the critical buckling load. Thus, buckling is strictly related to both snap and the blue-sky catastrophe phenomena. With the map in Fig. 4 and Inverse Kinematics, it is possible to exploit controlled R-SIP with a pick and place perspective.

V. Simulations

The proposed model and controller are validated through numerical examples. In the first example, R-SIP is modeled with CP, i.e. (9). The system is controlled by the control law (44) to a desired trajectory $\theta_{\text{rd}}(t)$ and is defined by the following parameters: $L = 1.0\,\text{m}$, $D = 0.1\,\text{m}$, $\rho(s) = m\,\delta(s-1)$, $m = 1.0\,\text{kg}$, $k = 1.0\,\text{Nm/rad}$, $k_{\text{r}} = 0.0\,\text{Nm/rad}$, $\beta = 0.1\,\text{Nms/rad}$, $\beta_{\text{r}} = 0.5\,\text{Nms/rad}$. Fig. 5(a), and (b), shows the results of simulations with $\theta_{\text{rd}}(t) = \arctan(t-15)$ and $\theta_{\text{rd}}(t) = \frac{\pi}{2}\,\delta_{-1}(t-15)$, respectively. Fig. 5(c), and (d) shows the final positions of R-SIP at the equilibrium $(\bar{\theta}_{\text{rd}}, \bar{q}_{\text{sip}})$, in which we can observe two different equilibria for the same $\bar{\theta}_{\text{rd}} = \frac{\pi}{2}$, confirming map showed in Fig. 4. An interesting fact is that, in the case of a discontinuous desired trajectory, the snap effect occurs, in contrast to the smooth one. This nonlinear behavior of the system can be exploited for pick and place purposes. An additional simulation is provided in the video attached to this work, with a sinusoidal reference trajectory.

Comparable results are obtained by simulating the SP model, as shown in Fig. 5(e)–(h). These simulations are computed with SoRoSim MATLAB toolbox [21]. The system is simulated with equivalent parameters, w.r.t. the previous simulations, such as with the following parameters: $L = 1.0\,\text{m}$, $D = 0.1\,\text{m}$, $\rho(X) = \bar{\rho}\,\delta(X - L)$, $\bar{\rho} = 1141.5728\,\text{kg/m}^3$, $E = 0.2037\,\text{MPa}$, $k_{\text{r}} = 0.0\,\text{Nm/rad}$, $\beta_{\text{r}} = 0.5\,\text{Nms/rad}$, $\beta = 0.0067906\,\text{MPas}$. The evolutions of the two models over time show a slight difference in the transient phase. This can be attributable to the different

discretization techniques employed. While the CP model derives an analytical solution from the integral (3), the SP model must numerically compute (18), introducing a numerical approximation that can cut high-frequency contributions.

A. Pick and Place Planner

Consider an R-SIP controlled by the law (44) and an object with a mass of m_{obj}. Assuming that R-SIP can grasp the object instantaneously without relative motion (e.g., suction cup mounted on the tip), we can describe the behavior of the entire system by increasing the value of the lumped mass on the robot's tip of $\Delta m = m_{\text{obj}}$. To model the *quasi-instantaneous* increase in load, we utilize a Sigmoid function, to avoid unrealistic discontinuous functions. Specifically, $\Delta m(t) = m_{\text{obj}}\,(1/(\exp(-a(t - t_{\text{act}}))))$, where t_{act} represents the time at which the R-SIP picks the object (e.g., activation time of the suction cup) and $a \in \mathbb{R}^+$ denotes the rate of the Sigmoid function. To exploit the snap effect for pick and place purposes, a planner has been developed. It consists of a sequence of desired trajectories $\theta_{\text{rd}}(t)$, designed to reach two desired equilibria and, consequently, two desired configurations. Fig. 6, shows a simulation of the controlled R-SIP with the pick and place planner, where $m_{\text{obj}} = 0.3\,\text{kg}$, $a = 4$ and $t_{\text{act}} = 40\,\text{s}$. To better visualize the planning strategy, Fig. 7 provides insight into the evolution of the system in the phase space, showcasing the planning strategy.

The strategy comprises three steps: in the first step (Fig. 6(a)), the desired trajectory is constant $\bar{\theta}_{\text{rd}} = \theta_{\text{rd}}^{(1)}$. The second step (Fig. 6(b)) consists in a slow linear trajectory $\theta_{\text{rd}} = -0.1(t - 40) + \theta_{\text{rd}}^{(1)}$ and the third step (Fig. 6(c)) returns to a constant $\bar{\theta}_{\text{rd}} = \theta_{\text{rd}}^{(2)}$. The first and third steps correspond to the "pick" and "place" phases, during which the soft manipulator grabs and releases the object. The value of $\theta_{\text{rd}}^{(1)}$ and $\theta_{\text{rd}}^{(2)}$ can be selected from the equilibria map, outside the region $[-\theta_{\text{rd}}^*(0),\ \theta_{\text{rd}}^*(0)]$ and $[-\theta_{\text{rd}}^*(m_{\text{obj}}),\ \theta_{\text{rd}}^*(m_{\text{obj}})]$, respectively. In the second step, the slow linear reference induces the snap effect. As shown in Fig. 7, the slowly varying $\theta_{\text{rd}}(t)$ guides the evolution of the system to follow the equilibria map of the robot with the object on its tip (Fig. 4), keeping the system in a quasi-static condition. When $\theta_{\text{rd}}\,(t) = \theta_{\text{rd}}^*(m_{\text{obj}})$, two equilibria vanish and R-SIP is attracted to the unique remaining equilibrium, causing a fast release of stored energy and a "*catapult-like trajectory*" [2].

VI. Conclusion

This letter introduced and analyzed the R-Soft Inverted Pendulum, including a comparative analysis of two equivalent formulations of the model. A Feedback Linearization control law has been designed to control this system. Moreover, a new strategy has been provided, exploiting the snap effect for the pick-and-place task. Finally, these theoretical elements have been validated through simulations, which showed the consistency of the models and the proposed controller. Future work will focus on the design and development of an R-SIP prototype to experimentally validate the system and the control law. In addition, a general pick and place strategy will be developed, using inverse kinematics and the equilibria map found in Section IV.

References

[1] D. Rus et al., "Design, fabrication and control of soft robots," *Nature*, vol. 521, no. 7553, pp. 467–475, May 2015.

[2] C. D. Santina, "The soft inverted pendulum with affine curvature," in *Proc. IEEE 59th Conf. Decis. Control*, 2020, pp. 4135–4142.

[3] S. Grazioso et al., "A geometrically exact model for soft continuum robots: The finite element deformation space formulation," *Soft Robot.*, vol. 6, no. 6, pp. 790–811, 2019.

[4] C. Armanini et al., "From the elastica compass to the elastica catapult: An essay on the mechanics of soft robot arm," *Proc. Roy. Soc. A: Math., Phys. Eng. Sci.*, vol. 473, no. 2198, Feb. 2017, Art. no. 20160870.

[5] C D. Santina and D. Rus, "Control oriented modeling of soft robots: The polynomial curvature case," *IEEE Robot. Automat. Lett.*, vol. 5, no. 2, pp. 290–298, Apr. 2020.

[6] F. Boyer, V. Lebastard, F. Candelier, and F. Renda, "Dynamics of continuum and soft robots: A strain parameterization based approach," *IEEE Trans. Robot.*, vol. 37, no. 3, pp. 847–863, Jun. 2021.

[7] F. Renda, C. Armanini, V. Lebastard, F. Candelier, and F. Boyer, "A geometric variable-strain approach for static modeling of soft manipulators with tendon and fluidic actuation," *IEEE Robot. Automat. Lett.*, vol. 5, no. 3, pp. 4006–4013, Jul. 2020.

[8] C. Armanini, F. Boyer, A. T. Mathew, C. Duriez, and F. Renda, "Soft robots modeling: A structured overview," *IEEE Trans. Robot.*, vol. 39, no. 3, pp. 1728–1748, Jun. 2023.

[9] C. D. Santina et al., "Model-based dynamic feedback control of a planar soft robot: Trajectory tracking and interaction with the environment," *Int. J. Robot. Res.*, vol. 39, no. 4, pp. 490–513, 2020.

[10] M. Pierallini et al., "A provably stable iterative learning controller for continuum soft robots," *IEEE Robot. Automat. Lett.*, vol. 8, no. 10, pp. 6427–6434, Oct. 2023.

[11] G. R. Fowles, *Introduction to Modern Optics*. Mineola, NY, USA: Dover Publications, 1975.

[12] A. H. Nayfeh et al. *Applied Nonlinear Dynamics: Analytical, Computational, and Experimental Methods*. Hoboken, NJ, USA: Wiley, Mar. 1995.

[13] M. Trumić, C. D. Santina, K. Jovanovi ć, and A. Fagiolini, "On the stability of the soft pendulum with affine curvature: Open-loop, collocated closed-loop, and switching control," *IEEE Control Syst. Lett.*, vol. 7, pp. 385–390, 2023.

[14] F. Stella, N. Obayashi, C. D. Santina, and J. Hughes, "An experimental validation of the polynomial curvature model: Identification and optimal control of a soft underwater tentacle," *IEEE Robot. Automat. Lett.*, vol. 7, no. 4, pp. 11410–11417, Oct. 2022.

[15] L. Weerakoon and N. Chopra, "Swing up control of a soft inverted pendulum with revolute base," in *Proc. IEEE 60th Conf. Decis. Control*, 2021, pp. 685–690.

[16] T. Burch, J. P. Lathrop, W. L. Scott, and D. A. Paley, "Feedback control of a soft swinging appendage," in *Proc. IEEE 3rd Int. Conf. Soft Robot.*, 2020, pp. 1–6.

[17] B. Siciliano et al. *Robotics: Modelling, Planning and Control*, 1st ed. London, U.K.: Springer, 2008.

[18] M. W. Spong, "Partial feedback linearization of underactuated mechanical systems," in *Proc. IEEE/RSJ Int. Conf. Intell. Robots Syst.*, 1994, pp. 314–321.

[19] F. Renda, M. Giorelli, M. Calisti, M. Cianchetti, and C. Laschi, "Dynamic model of a multibending soft robot arm driven by cables," *IEEE Trans. Robot.*, vol. 30, no. 5, pp. 1109–1122, Oct. 2014.

[20] F. Renda, M. Giorelli, M. Calisti, M. Cianchetti, and C. Laschi, "Discrete cosserat approach for soft robot dynamics: A new piece-wise constant strain model with torsion and shears," in *Proc. IEEE/RSJ Int. Conf. Intell. Robots Syst.*, 2016, pp. 5495–5502.

[21] A. T. Mathew, I. B. Hmida, C. Armanini, F. Boyer, and F. Renda, "SoRoSim: A MATLAB toolbox for hybrid rigid-soft robots based on the geometric variable-strain approach," *IEEE Robot. Automat. Mag.*, vol. 30, no. 3, pp. 106–122, Sep. 2023.

[22] M. Gazzola et al., "Forward and inverse problems in the mechanics of soft filaments," *Roy. Soc. Open Sci.*, vol. 5, no. 6, Jun. 2018, Art. no. 171628.

[23] R. M. Murray et al. *A Mathematical Introduction to Robotic Manipulation*, 1st ed., Boca Raton, FL, USA: CRC Press, Inc., 1994.

[24] E. Haier et al. *Geometric Numerical Integration: Structure-Preserving Algorithms for Ordinary Differential Equations*. New York, NY, USA: Springer, 2006.

[25] H. Khalil, *Nonlinear Systems*, (Pearson Education Series). Hoboken, NJ, USA: Prentice Hall, 2002.

[26] C. D. Santina, C. Duriez, and D. Rus, "Model-based control of soft robots: A survey of the state of the art and open challenges," *IEEE Control Syst. Mag.*, vol. 43, no. 3, pp. 30–65, Jun. 2023.

[27] M. P. d. Carmo, *Differential Geometry of Curves and Surfaces*. Hoboken, NJ, USA: Prentice Hall, 1976.